


Subcycle time-resolved nondipole dynamics in tunneling ionization

Michael Klaiber¹,* Karen Z. Hatsagortsyan¹,† and Christoph H. Keitel¹
Max-Planck-Institut für Kernphysik, Saupfercheckweg 1, 69117 Heidelberg, Germany

 (Received 9 March 2022; revised 11 April 2022; accepted 27 April 2022; published 10 May 2022)

The electron nondipole dynamics in tunneling ionization in an elliptically polarized laser field is investigated theoretically using a relativistic Coulomb-corrected strong-field approximation (SFA) based on the eikonal approximation of the Klein-Gordon equation. We calculate attoclock angle-resolved light-front momentum distributions at different ellipticities of the laser field in quasistatic and nonadiabatic regimes and analyze them with an improved simple man's model. The nondipole correlations between longitudinal and transverse momentum components are examined. Deviations of the nondipole photoelectron momentum distribution calculated via SFA with respect to the available experimental results as well as with the improved simple man's model are discussed and interpreted in terms of nonadiabatic as well as Coulomb effects in the continuum and under the barrier. The favorable prospects of an experimental observation are discussed.

DOI: [10.1103/PhysRevA.105.053107](https://doi.org/10.1103/PhysRevA.105.053107)

I. INTRODUCTION

High-precision measurements in strong-field atomic physics allow to detect nondipole features in photoelectron momentum distribution (PMD) at laser intensities far below the relativistic regime [1–12]. The leading nondipole effect in tunneling ionization is due to the laser magnetic field and results in imparting the photoelectron a momentum along the laser propagation direction, which has consequences for the partitioning of the absorbed photon momentum between the photoelectron and the parent ion [1,13–24]. The electron energy resolution of state-of-the-art detection techniques [25] is of about meV, which corresponds to a momentum resolution of about 0.01 a.u. The nondipole shift of a longitudinal momentum can be estimated as $p_k \sim ca_0^2$ [26], with the relativistic invariant laser field parameter $a_0 = E_0/(c\omega)$ [27], the laser field amplitude E_0 , frequency ω , and the speed of light c . Atomic units are used throughout if not specified otherwise. This means that a nondipole shift of a longitudinal momentum can be detected in a laser field with $a_0 \sim 10^{-2}$ corresponding to a laser intensity $I \sim 10^{14}$ W/cm² at 800-nm wavelength. With the recent advancement of the strong-field laser technique into the mid-infrared (mid-IR) region up to wavelengths of the order of 10 μ m [28], the nondipole effects become measurable at even lower laser intensities. The Lorentz force effect matters not only in the continuum but also during the subbarrier tunneling dynamics, inducing an

additional longitudinal momentum shift $I_p/(3c)$ [5,13], with the ionization potential I_p . The latter is increased by subbarrier Coulomb corrections [24].

In a linearly polarized laser field, the drift of the electron induced by the laser magnetic field is known to suppress the recollision and related phenomena (see, e.g., [29–31]). At restrained recollisions, the interplay between the Coulomb, ellipticity, and nondipole effects in the continuum induces specific structures in PMD [2–4,32–38]. In an elliptically polarized laser field close to circular the Coulomb field of the atomic core disturbs the photoelectron motion in the continuum mostly near the tunnel exit; however, it also modifies the subbarrier dynamics [24].

While in first experiments [1,5,6] the average of the longitudinal momentum shift was in the attention of investigation, the recent experiment of Ref. [4] provides a subcycle time-resolved study, and the experiment of Ref. [8] investigates nondipole correlations between longitudinal-transverse momentum components in the ionized wave packet. The nondipole effects have been observed also in high-order above-threshold ionization [9], and the photoelectron energy peaks shift against the radiation pressure has been shown in the experiment [10]. The results of these experiments have raised significant interest of theory, addressing different aspects of the nondipole phenomena, in particular investigating the nonadiabatic [39], and Coulomb effects [40,41], as well as the intercycle interference structure in the PMD in the nondipole regime [42,43]. Recently, the magnetic-field effect has been proposed to be used as a tool to monitor electron correlations in nonsequential double ionization [12].

In this paper we investigate theoretically the electron nondipole dynamics in an elliptically polarized laser field in detail. A relativistic strong-field approximation (SFA) is employed and Coulomb corrections in the continuum as well as during tunneling are included in the eikonal approximation. Main attention is devoted to the investigation of nondipole features of the attoclock angle-resolved light-front momentum

*klaiber@mpi-hd.mpg.de

†k.hatsagortsyan@mpi-hd.mpg.de

Published by the American Physical Society under the terms of the Creative Commons Attribution 4.0 International license. Further distribution of this work must maintain attribution to the author(s) and the published article's title, journal citation, and DOI. Open access publication funded by the Max Planck Society.

distribution and on possible nondipole correlations between longitudinal-transverse momentum components. The role of nonadiabatic and Coulomb effects in the continuum and during tunneling as well as their interplay are analyzed for the nondipole dynamics. The simple man's model [44] is improved, including nondipole, nonadiabatic, and Coulomb corrections, for an intuitive interpretation of the PMD features within the SFA theory. The light-front momentum as a choice for an observable is underlined as being especially suitable for exploring the role of nonadiabatic and Coulomb effects for modifying the characteristics of the nondipole dynamics. While the main aim of the paper is the investigation of all nondipole effects of the order of $1/c$, we apply a fully relativistic theory because it allows for a more consistent and compact treatment than the nondipole one.

II. THEORETICAL APPROACH

The tunneling ionization of a hydrogenlike ion in a strong laser field is investigated. We employ a relativistic Coulomb-corrected SFA (CCSFA) based on the Klein-Gordon equation, where the Coulomb potential of the atomic core is accounted for using the eikonal approximation [45,46]. The ionization amplitude is calculated in the dressed partition [47], neglecting small spin effects [48]:

$$m_{\mathbf{p}} = -i \int dt \langle \psi_{\mathbf{p}}(t) | H_i | \phi(t) \rangle \quad (1)$$

with the interaction Hamiltonian $H_i = \mathbf{r} \cdot \mathbf{E}(\eta)$. The laser field is elliptically polarized:

$$\mathbf{E} = -\frac{E_0}{\sqrt{1+\epsilon^2}} [\mathbf{e}_x \cos(\omega\eta) + \epsilon \mathbf{e}_y \sin(\omega\eta)], \quad (2)$$

where ϵ is the ellipticity, $\eta = t - \hat{\mathbf{k}} \cdot \mathbf{r}/c = t - z/c$, $\hat{\mathbf{k}}$ the unit vector along the laser propagation direction, $\phi(\mathbf{r}, t) = c_a \phi_0(\mathbf{r}, t) \phi_1(\mathbf{r}, t)$ is the initial bound state of the electron in the atomic Coulomb potential $V = -Z/r$, with charge Z and an asymptotic expression at $r \gg 1/\kappa$:

$$\phi_0(\mathbf{r}, t) = \frac{\exp(-\kappa r + i\kappa^2/2t)}{r}, \quad \phi_1(\mathbf{r}) = (\sqrt{2\kappa r})^{Z/\kappa}, \quad (3)$$

with $c_a \equiv \sqrt{\kappa/(2\pi)}$ and $\kappa = \sqrt{2I_p}$. We use the nonrelativistic bound state because the relativistic corrections scale as I_p/c^2 and are negligible for the applied conditions. The electron final state in the continuum is assumed to be the Coulomb-Volkov state in the eikonal approximation [46]:

$$\psi_{\mathbf{p}}(\mathbf{r}, t) = \frac{1}{(2\pi)^{3/2}} \exp[iS_0(\mathbf{r}, t) + iS_1(\mathbf{r}, t)]. \quad (4)$$

The applied eikonal approximation is valid if the momentum change of the electron due to the Coulomb field is smaller with respect to the electron momentum via the laser field. This is the case when hard recollisions do not play a role, which exactly corresponds to the electron dynamics discussed in this paper, namely, ionization in an elliptically polarized laser field with $\epsilon \gtrsim 0.3$ [3,33]. Here,

$$S_0(\mathbf{r}, t) = (\mathbf{p} + \mathbf{A}(\eta) - (\varepsilon/c - c)\hat{\mathbf{k}}) \cdot \mathbf{r} + \int_{\eta}^{\infty} ds [\mathcal{E}(s) - c^2]$$

is the Volkov action, $\varepsilon = \sqrt{c^4 + c^2 \mathbf{p}^2}$ the electron energy,

$$\mathbf{A}(\eta) = \frac{E_0/\omega}{\sqrt{1+\epsilon^2}} [\mathbf{e}_x \sin(\omega\eta) - \epsilon \mathbf{e}_y \cos(\omega\eta)] \quad (5)$$

is the laser vector potential, and

$$\mathcal{E}(s) = \varepsilon + \frac{\mathbf{p} \cdot \mathbf{A}(s) + \mathbf{A}(s)^2/2}{\Lambda} \quad (6)$$

is the electron energy in the laser field, with the integral of motion $\Lambda = \varepsilon/c^2 - p_k/c$ and $p_k = \hat{\mathbf{k}} \cdot \mathbf{p}$. Further, the Coulomb correction (CC) to the eikonal is

$$S_1(\mathbf{r}, t) = \int_{\eta}^{\infty} ds \frac{\mathcal{E}(s)}{\Lambda c^2} V(\mathbf{r}(s, \eta)), \quad (7)$$

with the electron relativistic trajectory

$$\mathbf{r}(\eta', \eta) = \mathbf{r} + \frac{1}{\Lambda} \int_{\eta}^{\eta'} ds \left(\mathbf{p} + \mathbf{A}(s) + \hat{\mathbf{k}} \frac{\mathbf{p} \cdot \mathbf{A}(s) + \mathbf{A}(s)^2/2}{c\Lambda} \right). \quad (8)$$

The ionization amplitude of Eq. (1) consists of a four-dimensional integral. After a coordinate transformation from t to η , we solve it with the four-dimensional saddle-point approximation (SPA). Deviating from common approaches, cylindrical coordinates are used $\mathbf{r} = (\rho, \varphi, z)$ (z axis along the laser propagation direction) for evaluation of the relativistic matrix element of strong-field ionization. The advantage is that the integrand is free of the singularity at $\mathbf{r} = 0$ in cylindrical coordinates and the SPA validity is mathematically justified. For the accurate application of SPA the integrand is exponentiated:

$$m_{\mathbf{p}} = -i \int d\eta d\rho d\varphi dz \exp(\zeta_0 + \zeta_1), \quad (9)$$

where $\zeta_0 = \ln(\rho c_a H_i \phi_0) - iS_0$ and $\zeta_1 = \ln(\phi_1) - iS_1$. Consequently, we obtain the saddle-point equations:

$$\begin{aligned} \partial_{\eta} \zeta_0(\rho, \varphi, z, \eta) &= 0, & \partial_{\rho} \zeta_0(\rho, \varphi, z, \eta) &= 0, \\ \partial_{\varphi} \zeta_0(\rho, \varphi, z, \eta) &= 0, & \partial_z \zeta_0(\rho, \varphi, z, \eta) &= 0. \end{aligned} \quad (10)$$

In the saddle-point equations it was assumed that the first-order term ζ_1 is slowly varying and therefore neglected with respect to the ζ_0 contribution. For a given final momentum \mathbf{p} the saddle-point equations are solved numerically, obtaining the ionization amplitude

$$m_{\mathbf{p}} = -i \sqrt{\frac{(-2\pi)^4}{\det \partial_i \partial_j \zeta_{0,s}}} \exp(\zeta_{0,s} + \zeta_{1,s}), \quad (11)$$

where indices i and j run over the cylindrical coordinates and η . The corresponding momentum distribution is then calculated via

$$\frac{dw(\mathbf{p})}{d^3\mathbf{p}} = |m(\mathbf{p})|^2. \quad (12)$$

III. SIMPLE MAN'S MODEL

In this section we extend the well-known simple man's model [44] into the relativistic domain for spinless particles and further improve it to include the nondipole subbarrier correction to the longitudinal momentum at the tunnel exit

and its CC, the nonadiabatic corrections to the initial electron momentum at the tunnel exit, as well as Coulomb corrections due to the continuum motion in the quasistatic and in nonadiabatic regimes. The improved simple man's model is a convenient tool for analyzing the role of the nonadiabatic and Coulomb effects in modifying the characteristics of the nondipole dynamics.

A. Quasistatic regime

In the simple man's model we find the most probable relativistic trajectory for the ionized electron, and accordingly the most probable asymptotic momentum corresponding to the peak of PMD in the nondipole regime. In the quasistatic regime the ionized electron appears in the continuum at the tunnel exit (at the laser phase $\phi_i = \omega\eta_i$) with a vanishing momentum $\mathbf{p}_{\perp i} = 0$, $p_{ki} = 0$. Here \mathbf{p}_{\perp} is the transverse momentum component in the polarization plane, and p_k the longitudinal component. Further, the electron moves in the laser and Coulomb fields of the atomic core.

First, we find the electron trajectory in a plane-wave laser field $\mathbf{A} = \mathbf{A}(\phi)$. In this field there are two relativistic integrals of motion following from the field symmetry, namely, from the field dependence only in the single variable ϕ :

$$\mathbf{p}_{\perp} - \mathbf{A}(\phi) = \mathbf{p}_{\perp i} - \mathbf{A}(\phi_i), \quad (13)$$

$$\varepsilon - cp_k = \varepsilon_i - cp_{ki} = c^2\Lambda, \quad (14)$$

with the initial energy ε_i at $\phi = \phi_i$, $\phi = \omega\eta$. From the latter the final photoelectron momentum is derived [see, e.g., Eq. (A10) in [3]]:

$$\mathbf{p}_{\perp} = \mathbf{p}_{\perp i} - \mathbf{A}(\phi_i), \quad (15)$$

$$p_k = p_{ki} + \frac{\mathbf{p}_{\perp}^2 - \mathbf{p}_{\perp i}^2}{2c\Lambda}. \quad (16)$$

Further, we use the relativistically correct expressions of Eqs. (15) and (16) for the nondipole regime [$O(1/c)$], when $\Lambda \approx 1 - p_{ki}/c \approx 1$. The latter can be expressed either via the initial transverse momentum $\mathbf{p}_{\perp i}$ or via the asymptotic one \mathbf{p}_{\perp} , which in the leading order of $O(1/c)$ reads as

$$p_k = p_{ki} - \frac{\mathbf{p}_{\perp i} \cdot \mathbf{A}(\phi_i) - A(\phi_i)^2/2}{c}, \quad (17)$$

$$p_k = p_{ki} - \frac{\mathbf{p}_{\perp} \cdot \mathbf{A}(\phi_i) + A(\phi_i)^2/2}{c}. \quad (18)$$

In the quasistatic regime and neglecting the subbarrier nondipole dynamics, $p_{ki} = 0$ and $\mathbf{p}_{\perp i} = 0$, and the peak of the final momentum distribution within the simple man's model is

$$\mathbf{p}_{\perp}^{(m)}(\phi_i) = -\mathbf{A}(\phi_i), \quad (19)$$

$$p_k^{(m)}(\phi_i) = \frac{p_{\perp}^{(m)}(\phi_i)^2}{2c}. \quad (20)$$

We define the light-front momentum via the integral of motion in a plane wave $p_- = c(1 - \Lambda)$:

$$p_- = p_k - \frac{\mathbf{p}_{\perp}^2}{2c}. \quad (21)$$

In the quasistatic simple man's picture the most probable value of the light-front momentum is, therefore, vanishing:

$$p_-^{(m)}(\phi_i) = 0. \quad (22)$$

The relationship of Eq. (22) for the time-resolved light-front momentum is fulfilled in a plane-wave laser field of any intensity and ellipticity as far as nonadiabatic and Coulomb effects, subbarrier nondipole effects, as well as recollisions are negligible. For this reason the momentum variable of $p_-(\phi_i)$ is a very convenient observable for the time-resolved investigation of signatures of nonadiabatic, subbarrier, and Coulomb effects in the nondipole dynamics. Note that recollisions do not play a significant role at rather large ellipticity of the laser field $\epsilon \gtrsim 0.3$ [3,33].

B. Subbarrier corrections

In this section we improve the simple man's model including the subbarrier nondipole, Coulomb, and nonadiabatic corrections. The subbarrier nondipole effects shift the peak of the longitudinal momentum distribution at the tunnel exit from the simple man's model value $p_{ki} = 0$ to

$$p_{ki} = \frac{I_p}{3c} \left[1 + 6\nu \frac{E(\phi_i)}{E_a} \right], \quad (23)$$

where the first term $I_p/(3c)$ is due to the subbarrier nondipole magnetic field effect [13], and the second term due to the subbarrier Coulomb field effect in the quasistatic and quasiclassical approximation [24], $\nu = Z/\kappa$ is the effective principal quantum number of the bound state, and $E_a = \kappa^3$ the atomic field strength.

In the nonadiabatic regime the peak of the transverse distribution in the polarization plane at the tunnel exit is shifted due to the action of the nonadiabatic transverse force $F_{\perp} \sim E'(\phi_i)\tau_K \sim \epsilon\gamma(\phi_i)E(\phi_i)$ with respect to the direction of the tunneling channel during the subbarrier dynamics within the Keldysh time $\tau_K = \gamma(\phi_i)/\omega$, with the Keldysh parameter $\gamma(\phi_i) = \omega\kappa/E(\phi_i)$. This yields a transverse nonadiabatic momentum shift [49]

$$\mathbf{p}_{\perp i}^{(nad)} = \frac{\epsilon\gamma(\phi_i)\kappa}{6} \hat{\mathbf{e}}_{\perp}(\phi_i), \quad (24)$$

where

$$\hat{\mathbf{e}}_{\perp}(\phi_i) = (E_y(\phi_i), -E_x(\phi_i))/E(\phi_i) \quad (25)$$

is the unit vector perpendicular to the time-dependent laser field.

C. Coulomb corrections in the continuum

During the continuum motion of the ionized electron, the Coulomb field of the atomic core induces a momentum transfer. In the case of large ellipticity $\epsilon \gtrsim 0.3$, recollisions are negligible and the Coulomb effect mostly arises during the electron motion near the tunnel exit with the coordinate $\mathbf{r}_e(\phi_i) = -I_p\mathbf{E}(\phi_i)/E(\phi_i)^2$.

While in the quasistatic limit the CCs at the tunnel exit are known [36,50], here we derive the CC including nonadiabatic effects. The CC to the momentum due to the atomic potential

$V(\mathbf{r})$ is calculated as follows:

$$\delta \mathbf{p}_C = - \int_{\eta_i}^{\infty} d\eta \nabla V(\mathbf{r}(\eta, \eta_i)), \quad (26)$$

using the electron trajectory $\mathbf{r}(\eta, \eta_i)$ in the laser field. The following results are obtained keeping the first-order nonadiabatic terms with respect to $\gamma(\phi_i)$ [valid at $\gamma(\phi_i) \ll 1$].

The CC to the momentum in the field direction reads as

$$\delta \mathbf{p}_{eC} = \pi Z \frac{\mathbf{E}(\phi_i)}{E_a} \left[1 + \frac{\gamma(\phi_i)}{3\pi} \frac{1 - \epsilon^2}{1 + \epsilon^2} \frac{E_0^2 \sin(2\phi_i)}{E(\phi_i)^2} \right], \quad (27)$$

where the first term coincides with the quasistatic Coulomb momentum transfer in the field direction derived in [50], which results in a rotation of the final PMD in the polarization plane, and inducing the attoclock offset angle $\delta\theta \sim \pi\omega Z/(\epsilon\kappa^3)$. The attoclock angle is defined via the transverse momentum components $\mathbf{p}_{\perp}^{(m)}(\phi_i) = (p_x^{(m)}(\phi_i), p_y^{(m)}(\phi_i))$ (in the polarization plane) of the PMD peak:

$$\tan \theta(\phi_i) = p_y^{(m)}(\phi_i)/p_x^{(m)}(\phi_i). \quad (28)$$

In the simple man's model the attoclock angle is $\theta_0 = \pi/2$, and the attoclock offset angle is defined as $\delta\theta = \theta - \theta_0$. The second term in Eq. (27) $\sim \gamma(\phi_i)$ is the nonadiabatic CC.

The CC to the momentum in the polarization plane, transverse to the field direction, is

$$\delta \mathbf{p}_{e\perp C} = - \frac{\epsilon\gamma(\phi_i)\kappa}{6} \frac{2Z}{\kappa} \frac{E(\phi_i)}{E_a} \left[1 + \frac{E_0^2}{E(\phi_i)^2(1 + \epsilon^2)} \right] \hat{\mathbf{e}}_{\perp}(\phi_i). \quad (29)$$

The first term is the CC due to the initial transverse nonadiabatic momentum following from [50]. The second term is an additional CC in the continuum due to the motion driven by the nonadiabatic transverse force $\delta p_{\perp} \sim \epsilon\gamma(\phi_i)\kappa$ (see the intuitive explanation in Appendix A).

The CC to the momentum in the laser propagation direction is

$$\delta p_{kC} = - \left(p_{ki} + \frac{I_p}{3c} \right) \frac{2Z}{\kappa} \frac{E(\phi_i)}{E_a} - \frac{3\pi}{16} \gamma(\phi_i) \frac{I_p}{3c} \frac{Z}{\kappa} \frac{E(\phi_i)}{E_a} \frac{1 - \epsilon^2}{1 + \epsilon^2} \frac{E_0^2 \sin(2\phi_i)}{E(\phi_i)^2}, \quad (30)$$

where the first term with the factor p_{ki} is the quasistatic Coulomb momentum transfer in the direction transverse to the field derived in [50], while the second term with the factor $I_p/(3c)$ is due to the electron nondipole displacement in the continuum by the $v \times B$ force (see the intuitive explanation in Appendix B), and the last term is the nonadiabatic CC.

Thus, taking into account the nondipole, Coulomb, and nonadiabatic effects under the barrier and in the continuum, we obtain the most probable initial momentum:

$$\mathbf{p}_{\perp i}^{(m)} = \pi Z \frac{\mathbf{E}(\phi_i)}{E_a} [1 + g_e(\phi_i)] + \frac{\epsilon\gamma(\phi_i)\kappa}{6} \hat{\mathbf{e}}_{\perp}(\phi_i) [1 - g_{\perp}(\phi_i)], \quad (31)$$

$$p_{ki}^{(m)} = \frac{I_p}{3c} \left[1 + 6\nu \frac{E(\phi_i)}{E_a} - g_k(\phi_i) \right], \quad (32)$$

with the nonadiabatic and Coulomb correction functions

$$g_e(\phi_i) = \frac{\gamma(\phi_i)}{3\pi} \frac{1 - \epsilon^2}{1 + \epsilon^2} \frac{E_0^2 \sin(2\phi_i)}{E(\phi_i)^2}, \quad (33)$$

$$g_{\perp}(\phi_i) = \frac{2Z}{\kappa} \frac{E(\phi_i)}{E_a} \left(1 + \frac{E_0^2}{E(\phi_i)^2(1 + \epsilon^2)} \right), \quad (34)$$

$$g_k(\phi_i) = \frac{E(\phi_i)}{E_a} \left[\frac{4Z}{\kappa} + \frac{3\pi}{16} \gamma(\phi_i) \frac{Z}{\kappa} \frac{1 - \epsilon^2}{1 + \epsilon^2} \frac{E_0^2 \sin(2\phi_i)}{E(\phi_i)^2} \right]. \quad (35)$$

Here we keep the leading terms in E_0/E_a , and have added the negative continuum Coulomb corrections to the initial momentum, assuming that it takes place during the motion near the tunnel exit in the case of a large ellipticity. With Eqs. (31) and (32) the most probable asymptotic momentum reads as

$$\mathbf{p}_{\perp}^{(m)}(\phi_i) = -\mathbf{A}(\phi_i) + \pi Z \frac{\mathbf{E}(\phi_i)}{E_a} [1 + g_e(\phi_i)] + \frac{\epsilon\gamma(\phi_i)\kappa}{6} \hat{\mathbf{e}}_{\perp}(\phi_i) [1 - g_{\perp}(\phi_i)], \quad (36)$$

$$p_k^{(m)}(\phi_i) = \frac{I_p}{3c} \left[1 + 6\nu \frac{E(\phi_i)}{E_a} - g_k(\phi_i) \right] + \frac{\mathbf{A}(\phi_i)^2}{2c} - \frac{\pi Z}{E_a} \frac{\mathbf{E}(\phi_i) \cdot \mathbf{A}(\phi_i)}{c} [1 + g_e(\phi_i)] - \frac{\epsilon\gamma(\phi_i)\kappa}{6} \frac{\hat{\mathbf{e}}_{\perp}(\phi_i) \cdot \mathbf{A}(\phi_i)}{c} [1 - g_{\perp}(\phi_i)]. \quad (37)$$

The mapping of the initial laser phase (ϕ_i) of the tunneled electron to the attoclock angle (θ) is derived from Eq. (28).

The light-front momentum (21) is an integral of motion:

$$p_{-}(\eta) = p_k(\eta) - \frac{p_{\perp}^2(\eta)}{2c} = p_{ki} - \frac{p_{\perp i}^2}{2c}. \quad (38)$$

From the latter, keeping the first-order terms with respect to E_0/E_a and γ , we have for the peak value of the asymptotic light-front momentum

$$p_{-}^{(m)}(\phi_i) = \frac{I_p}{3c} \left[1 + 6\nu \frac{E(\phi_i)}{E_a} - g_k(\phi_i) \right]. \quad (39)$$

The term $p_{\perp i}^2/(2c)$ in Eq. (38) has contributions of the order of $O((E_0/E_a)^2, \gamma^2)$, which are neglected.

Thus, we have derived in the weakly nonadiabatic regime the most probable asymptotic momentum of the photoelectron within the simple man's model [Eqs. (36) and (39)], which provides the parametric dependence of the asymptotic momentum on the attoclock angle θ via the parameter ϕ_i [Eq. (28)]. The estimation for the light-front momentum (39) includes the nondipole subbarrier momentum shift ($I_p/3c$), quasistatic CC during the subbarrier dynamics [$6\nu E(\phi_i)/E_a$] and in the continuum [$(-4Z/\kappa)E(\phi_i)/E_a$], as well as nonadiabatic CC [$\sim \gamma(\phi_i)2Z/\kappa$]. The estimation for the transverse momentum (36) includes the quasistatic CC during the continuum dynamics [$\pi Z E(\phi_i)/E_a$], and its nonadiabatic correction [$\sim \gamma(\phi_i)$] as well as the nonadiabatic momentum shift due to subbarrier dynamics [$\epsilon\gamma(\phi_i)\kappa/6$], and its CC ($\sim (2Z/\kappa)[E(\phi_i)/E_a]$).

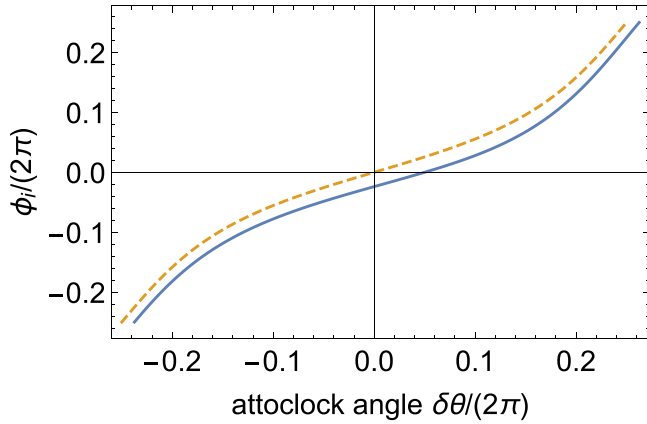


FIG. 1. Ionization phase ϕ_i vs attoclock offset angle $\delta\theta$ via the improved simple man's model (28) (blue, solid), and plain simple man's model (orange, dashed). The laser field strength is $E_0 = 0.05$, frequency $\omega = 0.05$, and ellipticity $\epsilon = 0.5$.

IV. COMPARISON OF SFA RESULTS WITH IMPROVED SIMPLE MAN'S MODEL

A. Time-resolved light-front momentum

In this section we consider the ellipticity dependence of the time-resolved light-front momentum $p_-(\phi)$ corresponding to the peak of PMD in the quasistatic and nonadiabatic regimes, respectively [for simplicity of notation we remove the superscript (m) in $p_-^{(m)}(\phi)$]. The use of the light-front momentum for the presentation of the results is quite useful because it immediately demonstrates the role of Coulomb and nonadiabatic corrections, as in the plain simple man's model $p_- = 0$. We note that in the nonrelativistic limit ($c \rightarrow \infty$) the light-front momentum p_- is vanishing exactly, as Eq. (39) indicates. We will present the p_- dependence on the attoclock offset angle $\delta\theta$ because the latter is of experimental significance. However, in the simple man's model [Eq. (39)] the dependence on the initial phase ϕ_i is derived, therefore, we first discuss the relation of the ionization phase to the attoclock offset angle (see Fig. 1). When the ionization phase varies within the half of the laser cycle $-\pi/2 \leq \phi_i \leq \pi/2$, the offset angle changes within $-0.4\pi \leq \delta\theta \leq 0.4\pi$. An important feature of Fig. 1 is that the peak of the laser field $\phi_i = 0$ is shifted from zero offset angle, i.e., the field is not symmetric with respect to $\delta\theta = 0$. It is due to the nonadiabatic Coulomb effects in the continuum.

In Fig. 2 the p_- dependence on the attoclock offset angle is presented. We have applied several versions of SFA: (1) full CCSFA, which includes all Coulomb corrections, i.e., during the subbarrier dynamics, as well as in the continuum; (2) tunnel Coulomb-corrected SFA (TCSFA), i.e., the SFA with only subbarrier Coulomb corrections; (3) plain SFA with no Coulomb corrections. We provide also a comparison of the SFA results with the improved simple man's model [Eq. (39)]. The general observation from the results of Fig. 2 is the following. In the quasistatic regime (in our example $\gamma \approx 0.4$), the improved simple man's model and the plain SFA describe quite well the full CCSFA results for the given ellipticity range $\epsilon = 0.5-0.9$. They both underestimate the CCSFA result for p_- slightly. The deviation of CCSFA result from the improved simple man's model and the plain SFA is not large because the

subbarrier CC (highlighted via TCSFA) and the continuum CC (included in CCSFA), which are of opposite sign and larger at small ellipticity values, compensate each other to some extent [24].

In the nonadiabatic regime [in our example $\gamma \approx 1.1$, Fig. 2 (right column)] there are large deviations of the plain SFA with respect to CCSFA at small ellipticity. The performance of the improved simple man's model is also not good. In the simple man's model we expand the nonadiabatic CC with respect to γ , and the model is not accurate at large γ . Nevertheless, we probe the improved simple man's formulas for the $\gamma \sim 1$ domain in Fig. 2. They do not predict the slope for the CCSFA result, and there is a deviation from CCSFA in the offset-angle dependence. The deviation is larger at small ellipticities and at large positive offset angles. The improved simple man's model does not capture this latter feature. This stems from nonadiabatic Coulomb corrections, which are larger for small ellipticity. In the nonadiabatic regime the electron stays longer near the core than the quasistatic estimation assumes, leading to a large CC. The characteristic feature of the CC in the nonadiabatic regime is that it induces an asymmetry between the positive and negative offset angles. At $\gamma \sim 1$ this effect is significant.

Contributions of different Coulomb and nonadiabatic corrections are analyzed in Fig. 3 for the nonadiabatic regime. The simple man's model without CC (but with nonadiabatic corrections) coincides with the plain SFA result for the time-resolved light-front momentum. The subbarrier and continuum CCs are underestimated by the simple man's model because of the applied expansion over γ parameter (weakly nonadiabatic approximation). This results in the final deviation of the improved simple man's model with respect to CCSFA. Especially the asymmetry of p_- with respect to the sign of the offset angle, which is due to the nonadiabatic Coulomb effects in the continuum, is not captured in the simple man's model. This asymmetry we have already seen in Fig. 1. We note that due to applied eikonal approximation in CCSFA, the CC effect sometimes becomes overestimated.

B. Transverse-momentum distribution resolved in time and in longitudinal momentum

In the previous section we investigated the absolute peak value of the time-resolved light-front momentum [Eq. (39)]. Following the experiment [8], we further provide a more detailed description and examine the peak of the transverse momentum distribution resolved in the longitudinal momentum, as well as resolved in time (attoclock offset angle). For a given ionization phase ϕ_i , let us fix p_k and calculate the maximum of the transverse momentum distribution with respect to the transverse momentum p_\perp . The final distribution over transverse momenta arises because of the deviation of the electron transverse momentum at the tunnel exit from the peak value given by Eqs. (31) and (32):

$$\mathbf{p}_{\perp i} = \mathbf{p}_{\perp i}^{(m)} + \hat{\mathbf{e}}_{\perp}(\phi_i)\tilde{p}_{\perp}, \quad (40)$$

$$p_{ki} = p_{ki}^{(m)} + \tilde{p}_k. \quad (41)$$

Then, taking into account the additional CCs due to the additional initial momenta $\tilde{p}_{\perp}, \tilde{p}_k$ we have from Eqs. (15)

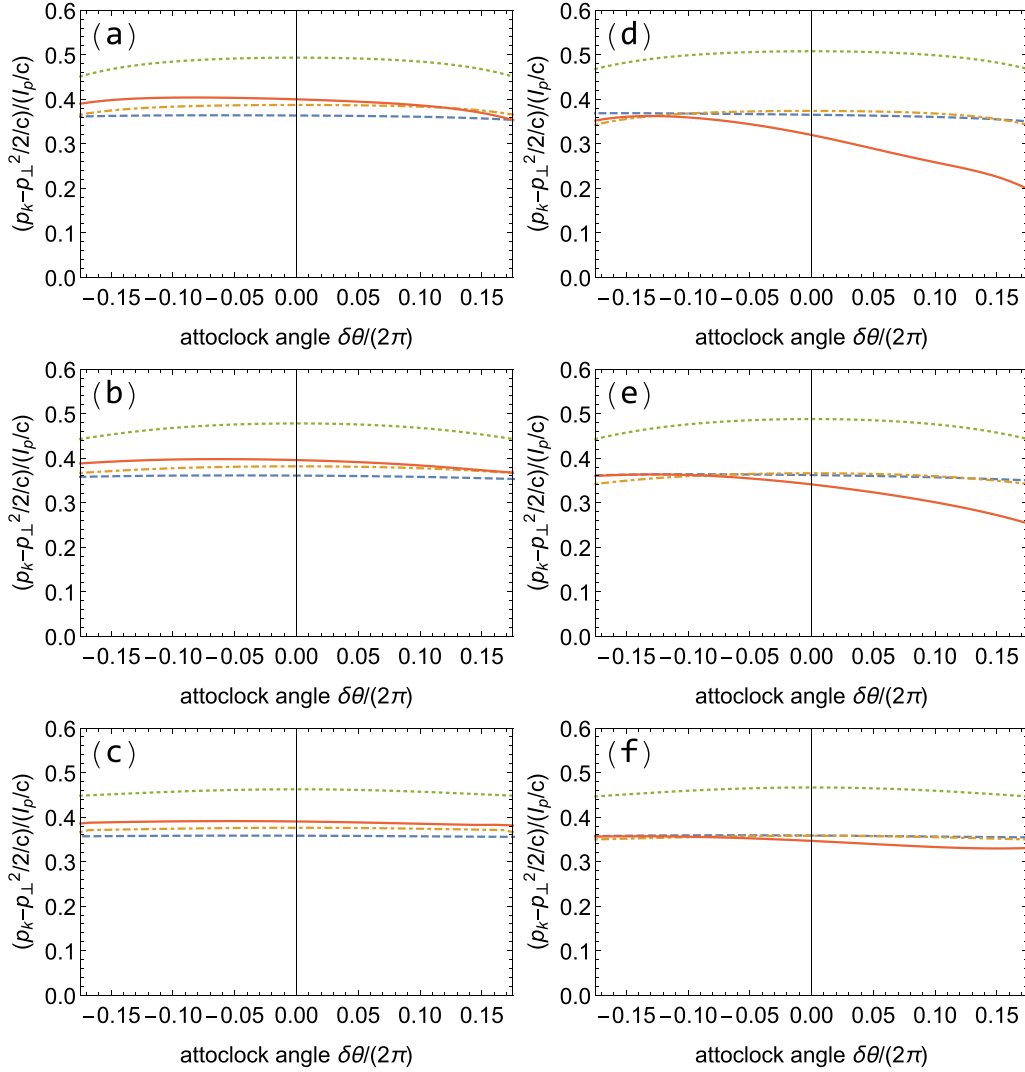


FIG. 2. Light-front momentum $p_- = p_k - \frac{p_\perp^2}{2c}$ vs attoclock offset angle $\delta\theta$. Left column: quasistatic regime, $\omega = 0.02$ ($\gamma \approx 0.4$); right column: nonadiabatic regime $\omega = 0.05$ ($\gamma \approx 1.1$); for ellipticity values (a), (d) $\epsilon = 0.5$, (b), (e) $\epsilon = 0.7$, (c), (f) 0.9 ; (red solid) CCSFA, (orange dashed-dotted) plain SFA without CC, (green dotted) TCSFA (SFA with only subbarrier CC), (blue dashed) improved simple man's model. The laser field strength is $E_0 = 0.05$. Note that in the nonrelativistic limit ($c \rightarrow \infty$) $p_- = 0$ exactly.

and (17)

$$\mathbf{p}_\perp = \mathbf{p}_\perp^{(m)}(\phi_i) + \hat{\mathbf{e}}_\perp(\phi_i) \tilde{p}_\perp [1 - g_\perp(\phi_i)], \quad (42)$$

$$p_k = p_k^{(m)}(\phi_i) + \tilde{p}_k [1 - g_k(\phi_i)] - \frac{\tilde{\mathbf{p}}_\perp \cdot \mathbf{A}(\phi_i)}{c} [1 - g_\perp(\phi_i)], \quad (43)$$

where $\mathbf{p}_\perp^{(m)}(\phi_i)$, $p_k^{(m)}(\phi_i)$ are the most probable asymptotic momentum components of the ionized wave packet at the tunnel exit via Eqs. (36) and (37). The factors $g_\perp(\phi_i)$, $g_k(\phi_i)$ account for the continuum CC due to the additional momentum \tilde{p}_k , \tilde{p}_\perp . Equation (43) shows that \tilde{p}_k and $\tilde{\mathbf{p}}_\perp$ are not independent at a given asymptotic momentum p_k :

$$\tilde{p}_\perp = \frac{[\mathbf{p}_\perp - \mathbf{p}_\perp^{(m)}(\phi_i)] \cdot \hat{\mathbf{p}}_\perp^{(m)}(\phi_i)}{[\hat{\mathbf{e}}_\perp(\phi_i) \cdot \hat{\mathbf{p}}_\perp^{(m)}(\phi_i)][1 - g_\perp(\phi_i)]}, \quad (44)$$

$$\tilde{p}_k = \frac{p_k - p_k^{(m)}(\phi_i)}{1 - g_k(\phi_i)} + \tilde{p}_\perp \frac{A_\perp(\phi_i)}{c} \frac{1 - g_\perp(\phi_i)}{1 - g_k(\phi_i)}, \quad (45)$$

where $A_\perp(\phi_i) = \mathbf{A}(\phi_i) \cdot \hat{\mathbf{e}}_\perp(\phi_i)$, and $\hat{\mathbf{p}}_\perp^{(m)}(\phi_i) \equiv \mathbf{p}_\perp^{(m)}(\phi_i)/|\mathbf{p}_\perp^{(m)}(\phi_i)|$. The probability distribution over electron momenta at the tunnel exit \tilde{p}_\perp , \tilde{p}_k is determined by the tunneling Perelomov-Popov-Terent'ev (PPT) distribution [51,52]

$$w(\tilde{p}_\perp, \tilde{p}_k) \propto \exp \left\{ -\frac{2}{3} \frac{(\kappa^2 + \tilde{p}_\perp^2 + \tilde{p}_k^2)^{3/2}}{E(\phi_i)} \right\} \\ \equiv \exp \{-G(\tilde{p}_\perp, \tilde{p}_k)\}.$$

Therefore, the maximum of the distribution for a given $p_k - p_k^{(m)}(\phi_i)$ is determined by the minimum of $G(\tilde{p}_\perp, \tilde{p}_k)$. From the condition

$$\partial G / \partial \tilde{p}_\perp = 0, \quad (46)$$

taking into account Eqs. (44) and (45), and keeping the terms linear in \tilde{p}_\perp , \tilde{p}_k , and up to the order of $1/c$, one obtains that a given $p_k - p_k^{(m)}(\phi_i)$, the transverse-momentum distribution is

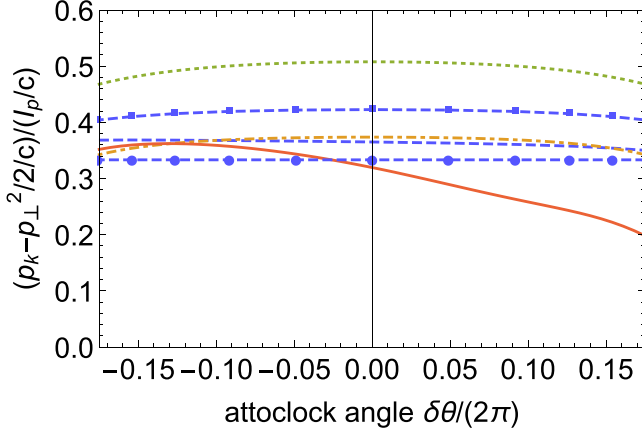


FIG. 3. (a) Different contributions to the simple man's model for the nonadiabatic regime, with $\omega = 0.05$ and ellipticity $\epsilon = 0.5$: (red, solid) CCSFA, (orange dashed-dotted) plain SFA without CC, (green dotted) TCSFA (no continuum CC), (blue dashed) improved simple man's model with all corrections, (blue dashed cycles) simple man's model with no continuum CC, (blue dashed boxes) simple man's model with no CC. The laser field strength is $E_0 = 0.05$.

maximal at

$$p_{\perp}(\phi_i) - p_{\perp}^{(m)}(\phi_i) = \alpha_{\phi_i} [p_k(\phi_i) - p_k^{(m)}(\phi_i)] \frac{A_0}{c}, \quad (47)$$

with $p_{\perp}(\phi_i) - p_{\perp}^{(m)}(\phi_i) \equiv [\mathbf{p}_{\perp}(\phi_i) - \mathbf{p}_{\perp}^{(m)}(\phi_i)] \cdot \hat{\mathbf{p}}_{\perp}^{(m)}(\phi_i)$, and the coefficient α_{ϕ_i} defined as

$$\alpha_{\phi_i} \equiv -\frac{A_{\perp}(\phi_i)}{A_0[\hat{\mathbf{e}}_{\perp}(\phi_i) \cdot \hat{\mathbf{p}}_{\perp}^{(m)}(\phi_i)]} \left[\frac{1 - g_{\perp}(\phi_i)}{1 - g_k(\phi_i)} \right], \quad (48)$$

and CC factors $g_{\perp}(\phi_i)$, $g_k(\phi_i)$ from Eqs. (34) and (35). Thus, the time-resolved PMD with respect to $(p_{\perp}(\phi_i), p_k(\phi_i))$ shows a local maximum, which runs along the line of Eq. (47). It is in accordance of the experimental observation of Ref. [8]: when $p_k > p_k^{(m)}$, one has a local maximum of p_{\perp} at a given p_k , which exceeds the absolute maximum $p_{\perp}^{(m)}$, and vice versa. An alternative derivation of the correlation of the transverse and longitudinal components momentum is given in Appendix C.

The correlation of the transverse and longitudinal momentum components given by Eq. (48) is time resolved via the ionization phase ϕ_i . However, it is not suitable for a direct experimental observation because in an experiment the PMD is time resolved via the attoclock angle θ . While there is a θ - ϕ_i relationship [Eq. (28)], it is momentum dependent, and the correlation (48) is not equivalent, though quite similar, to the experimentally accessible relationship

$$p_{\perp}(\theta) - p_{\perp}^{(m)}(\theta) = \alpha_{\theta} [p_k(\theta) - p_k^{(m)}(\theta)] \frac{A_0}{c}, \quad (49)$$

where $p_{\perp}(\theta)$ is the most probable transverse momentum at the given offset angle θ , and $p_{\perp}^{(m)}(\theta)$ its peak value, $A_0 = \epsilon E_0 / (\omega \sqrt{1 + \epsilon^2})$. This is because for the given attoclock angle θ , the corresponding ϕ_i is different for $p_{\perp}^{(m)}$ and p_{\perp} .

While in Eq. (49) we parametrize by α_{θ} the correlation between the deviations of the most probable transverse momentum $p_{\perp}(\theta)$ and the longitudinal momentum $p_k(\theta)$ from

the global most probable corresponding values of $p_{\perp}^{(m)}(\theta)$ and $p_k^{(m)}(\theta)$, in Ref. [8] the coefficient α parametrizes the relationship of the deviation of the average of the transverse momentum $\langle p_{\perp} \rangle$ (with respect to the simple man value $p_{\perp}^{(m)} = A_0$) to that of p_k (with respect to the simple man's model value $p_k^{(m)} = 0$): $\alpha = (p_{\perp} - A_0) / (p_k A_0 / c)$.

In Fig. 4 we show the time-resolved dependence of the α_{θ} parameter on the ellipticity of the laser field. First of all, there is no significant CC effect in the quasistatic regime [Figs. 4(a)–4(c)], especially at large ellipticities, as the results of the plain SFA, TCSFA, and CCSFA are very close to each other. In the nonadiabatic regime [Figs. 4(d)–4(f)] we note that there is no significant effect of subbarrier CC, as TCSFA results coincide with the plain SFA at any ellipticity. However, a significant deviation of CCSFA results from the plain SFA is observed in the nonadiabatic regime at small ellipticity and large positive offset angles, induced by the nonadiabatic CC in the continuum. There is an asymmetry in α with respect to the sign of the offset angle due to nonadiabaticity. A comparison of the SFA results for α_{θ} with the improved simple man's model α_{ϕ_i} indicates that the equivalence of α_{θ} to α_{ϕ_i} in both regimes is broken at small ellipticities and large offset angles. Note also that $\alpha_{\phi_i} = 1$ for the simple man's model at $\delta\theta = 0$, but α_{ϕ_i} is increasing at large offset angles.

In Fig. 5 we present the field dependence of the α parameter. As expected, for the plain SFA $\alpha_{\theta} = 1$ at any ellipticity and intensity. There is a remarkable influence of the continuum CC, which increases significantly the α_{θ} parameter in weak fields and at small ellipticities. The simple man's model does not fully account CC, especially nonadiabatic CC in the continuum.

V. LONGITUDINAL MOMENTUM AT SMALL ELLIPTICITY VALUES: ROLE OF RECOLLISIONS

The improved simple man's model presented in Sec. III fails for small ellipticity values. In this case recollisions play a role and we have no analytical expression to account for the recollision effect. In this section we put forward an augmentation of the improved simple man's model to account for the recollision effect approximately, and check its capability for small ellipticity values. The augmentation is straightforward: For the most probable trajectory we calculate the final longitudinal momentum of the electron numerically within a classical consideration, assuming initial conditions at $\phi_i = 0$ according to the improved simple man's model:

$$p_{xi} = 0, \quad p_{yi} = \epsilon \gamma(\phi_i) \kappa / 6, \quad p_{ki} = I_p / (3c), \quad (50)$$

and the initial coordinate at the tunnel exit

$$\mathbf{r}_e = -\hat{\mathbf{e}}(\phi_i) I_p / E(\phi_i). \quad (51)$$

With these initial conditions Newton equations are integrated assuming the Coulomb field as a perturbation:

$$p_k = p_{ki} - \frac{\mathbf{p}_{\perp i} \cdot \mathbf{A}(\phi_i) - A(\phi_i)^2 / 2}{c} - \int_{\eta_i}^{\infty} d\eta \partial_z V(\mathbf{r}(\eta, \eta_i)), \quad (52)$$

with $\eta_i = \phi_i / \omega$. In Fig. 6 we show the ellipticity dependence of the most probable longitudinal momentum, calculated via

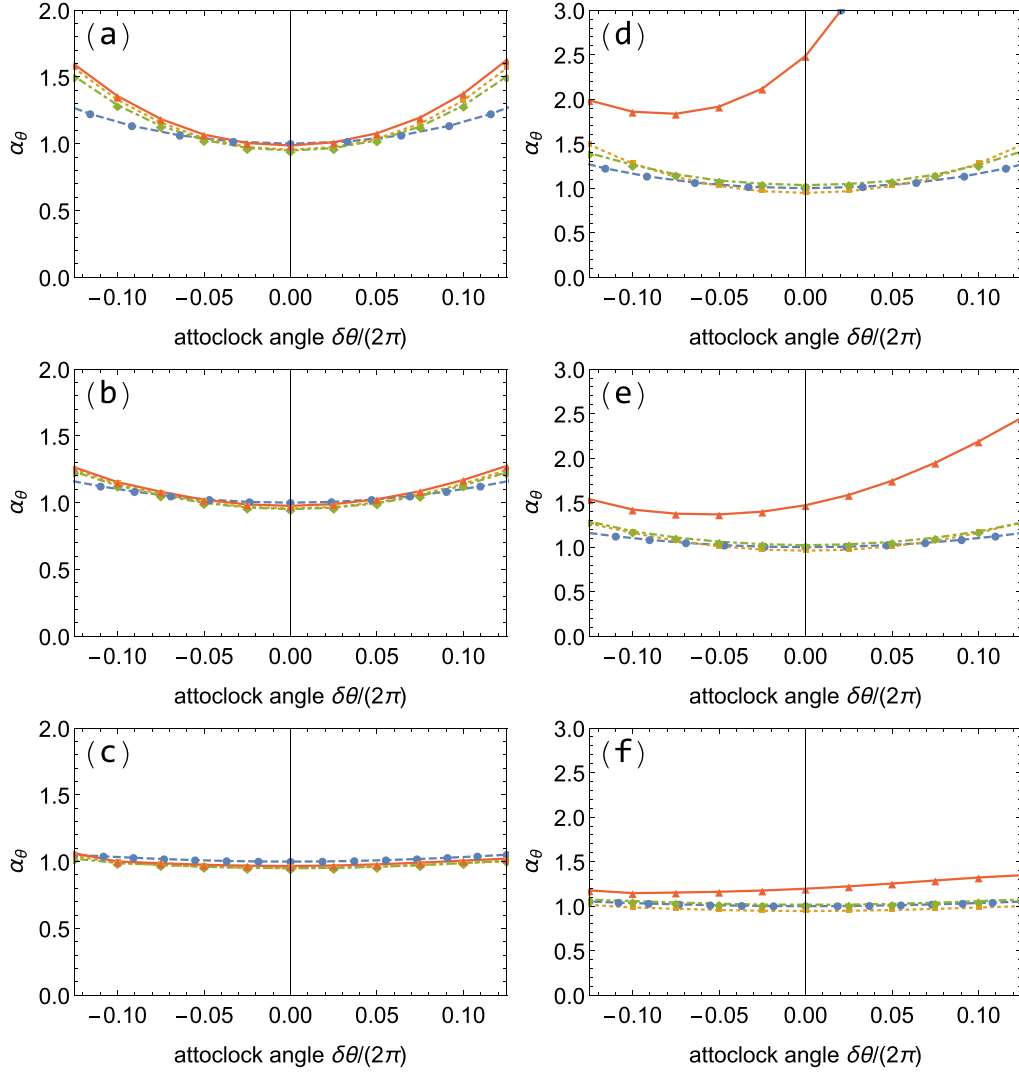


FIG. 4. The coefficient α_θ from Eq. (49) vs attoclock offset angle $\delta\theta$. Left column: quasistatic regime, $\omega = 0.02$ ($\gamma \approx 0.4$); right column: nonadiabatic regime $\omega = 0.05$ ($\gamma \approx 1.1$); for ellipticity values (a), (d) 0.5, (b), (e) 0.7, (c), (f) $\epsilon = 0.9$; (red solid) CCSFA, (orange dashed-dotted) plain SFA without CC, (green dotted) TCSFA (SFA with only subbarrier CC), (blue dashed) improved simple man's model. The laser field strength is $E_0 = 0.05$.

the augmented simple man's estimation. Surprisingly, such a simple model predicts quite correctly the ellipticity value ($\epsilon = 0.12$) when the most probable longitudinal momentum vanishes $p_k = 0$. From Fig. 3(a) of the experimental result of Ref. [3], this ellipticity value is $\epsilon = 0.11$. However, this simple model does not account for the phase-space deformation due to the Coulomb focusing effect, and correspondingly fails at smaller ellipticities, when this effect essentially modifies the PMD.

VI. EXPERIMENTAL TIME-RESOLVED SPECTRA VS CCSFA

In this section we compare the CCSFA calculations of the time-resolved nondipole momentum shift to the experimental data of Ref. [4]. In the latter, rather than the light-front momentum, the data for the longitudinal momentum are presented as a function of the so-called streaking angle. In

contrast to the attoclock angle defined by Eq. (37) in Cartesian coordinates, the streaking angle $\theta_{\text{elliptical}}$ is defined using elliptical coordinates. The relation between the elliptical coordinates $\theta_{\text{elliptical}}$, p_ρ , p_z and the Cartesian one (p_x , p_y , p_z) is

$$\theta_{\text{elliptical}} = \frac{1}{f} \text{Im}\{\cosh^{-1}(p_x - ip_y)\}, \quad (53)$$

$$p_\rho = \frac{1}{f} \text{Re}\{\cosh^{-1}(p_x - ip_y)\}, \quad (54)$$

$$p_z = p_z, \quad (55)$$

with $f = \sqrt{1 - \epsilon^2(E_0/\omega)}$, and the inverse mapping

$$p_x = f \cosh(p_\rho) \cos(\theta_{\text{elliptical}}), \quad (56)$$

$$p_y = -f \cosh(p_\rho) \sin(\theta_{\text{elliptical}}), \quad (57)$$

$$p_z = p_z, \quad (58)$$

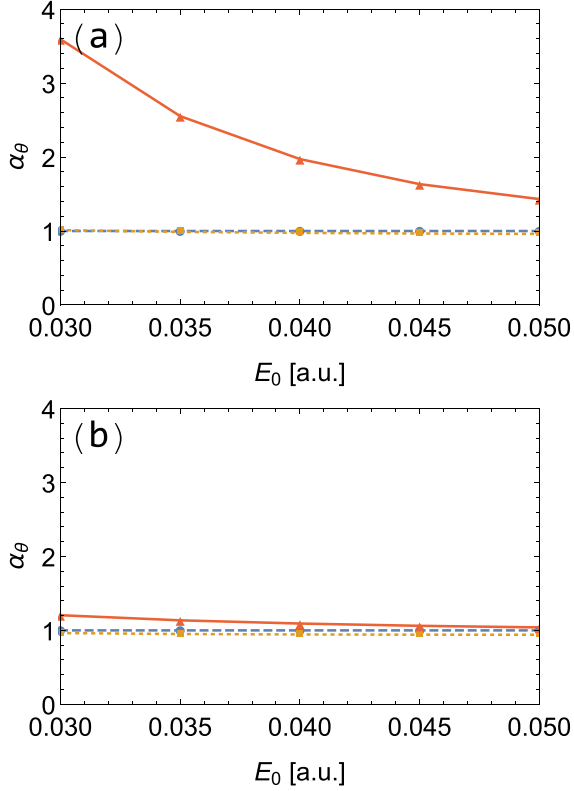


FIG. 5. The coefficient α_θ [Eq. (49)] (at $\delta\theta = 0$) vs the laser field, for $\omega = 0.04$ a.u. and $\kappa = 1$ a.u.: (a) $\epsilon = 0.6$; (b) $\epsilon = 1$; (red solid) CCSFA, (orange dashed-dotted) plain SFA without CC, (blue dashed) improved simple man's model.

which allows a linear relationship between the ionization phase and the streaking angle.

In Fig. 7 we show the offset angle, expressed as a time delay, between the attoclock angle of the maximum yield and the minimum of the longitudinal momentum vs ellipticity. Both the simple man's model and CCSFA results are in accordance with the experimental data within the error bars. However, the experimental data hint for a slight slope decreasing the time delay at large fields. This feature is absent in the simple man's model, but demonstrated by CCSFA.

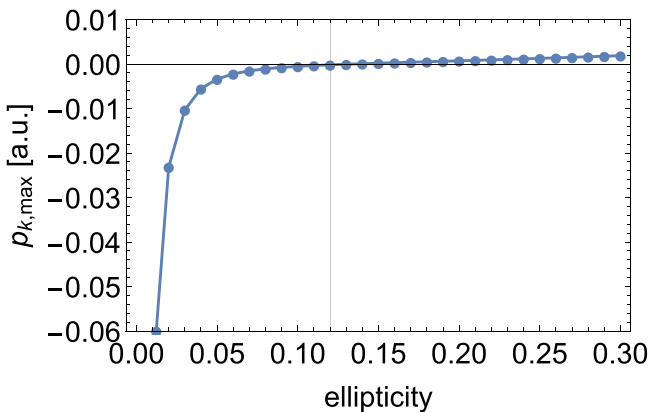


FIG. 6. The most probable longitudinal momentum via the augmented simple man's model (with forward rescattering) vs ellipticity, for $\omega = 0.01345$ a.u., $\kappa = 0.944$ a.u., and $E_0 = 0.0338$ a.u.

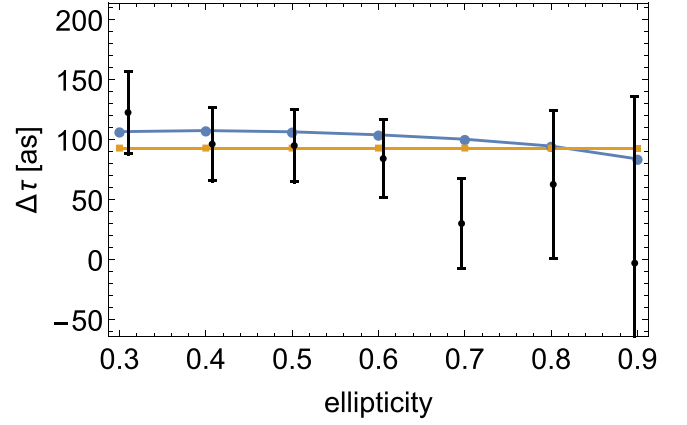


FIG. 7. Offset angle (expressed as a time delay) between the attoclock angle of the maximum yield and the minimum of the longitudinal momentum vs ellipticity. Experimental data [4] with error bars are black, CCSFA (blue cycles) and simple man's model results (orange boxes).

In Fig. 8 the CCSFA and simple man's model results for the average of the longitudinal momentum vs the elliptical offset angle $\delta\theta_{\text{elliptical}} = -\phi_i + \pi/2$ are compared with the experiment. The simple man's model results on the time-resolved data coincide with those of CCSFA; however, there are significant deviations with respect to the experiment, especially at large offset angles. However, the qualitative features of the curves, as in the simple man's approximation, in SFA, as well as in the experiment, coincide. Namely, the value of $\langle p_k \rangle$ at $\delta\theta = 0$ decreases with the decrease of the ellipticity, and increases with the increase of $|\delta\theta|$ at a fixed ellipticity (the increase is larger at small ellipticity). Both features can be explained via Eq. (37), where the main contribution at the given parameters comes from the second and fourth terms, the ponderomotive drift term $\mathbf{A}^2/(2c)$ and the nondipole drift term $\epsilon\gamma(\phi_i)[- \hat{\mathbf{e}}_\perp(\phi_i) \cdot \mathbf{A}(\phi_i)]\kappa/(6c) = \epsilon a_0 \kappa^2/[6E(\phi_i)]$, respectively, with both terms positive. We note that $A(\phi_i) \propto \sqrt{1 - (1 - \epsilon^2) \cos^2 \phi_i}$ increases with the larger offset angles, and the increase is larger at smaller ellipticity; $E(\phi_i) \propto \sqrt{1 - (1 - \epsilon^2) \sin^2 \phi_i}$ decreases with the larger offset angles, and the decrease is larger at smaller ellipticity. With this information, we can deduce that at $\delta\theta = 0$ the ponderomotive and the nondipole drift terms' contribution in $\langle p_k \rangle$ decreases at smaller ellipticity. At a given ellipticity, the increase of $|\delta\theta|$ will increase both drift terms and $\langle p_k \rangle$, where the increase is larger at smaller ellipticity. Thus, the mentioned two qualitative features of the $\langle p_k \rangle$ dependence can be explained with the ponderomotive and nondipole drifts. While the improved simple man's model captures these qualitative features, it underestimates the nonadiabatic effect at weak fields (large offset angles). Note that the subbarrier and the continuum CCs compensate each other, as the first is positive and the second negative. Our CCSFA result in Fig. 8 is closer to the experimental spectra than the classical Monte Carlo trajectory simulations (CTMC) of Ref. [4]. The reason could stem from the above-mentioned compensation of CCs in the continuum and under the barrier, along with the neglect of the subbarrier CC and nonadiabatic effects in CTMC.

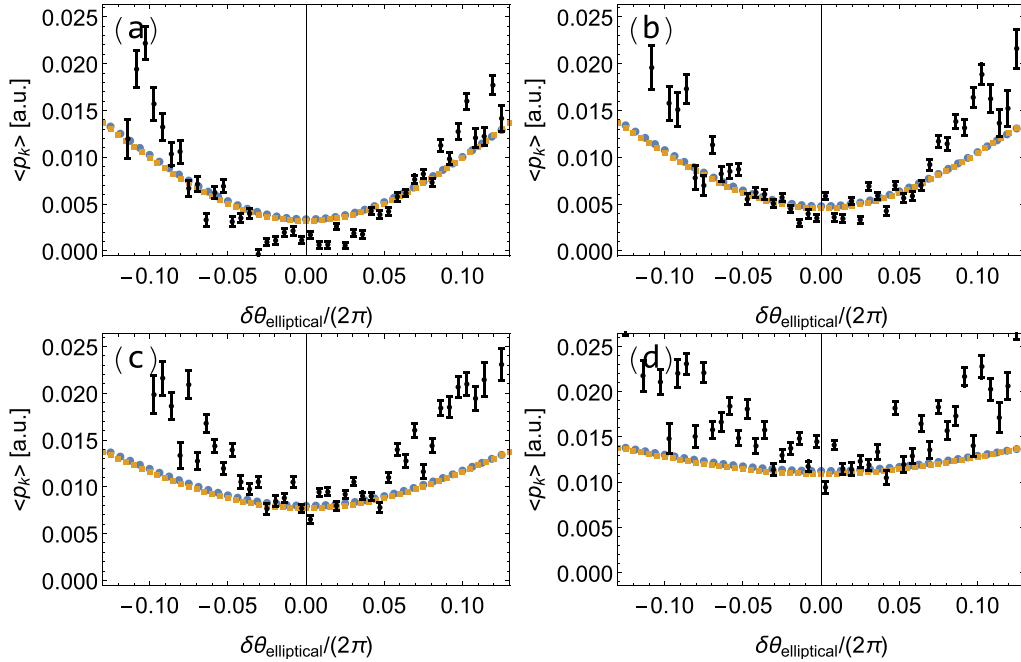


FIG. 8. The average longitudinal momentum $\langle p_k \rangle$ vs the streaking elliptical offset angle: (a) $\epsilon = 0.3$; (b) $\epsilon = 0.4$; (c) $\epsilon = 0.6$; (d) $\epsilon = 0.8$. Experimental data [4] with error bars are black; CCSFA (blue cycles) and simple man's model results (orange boxes).

In Fig. 9 we compare the results of CCSFA for the dependence of the average of the longitudinal momentum on the transverse one with the experimental data of Ref. [5]. Generally, the Coulomb corrections are not very significant for the given interaction regime. However, we note an important message of Fig. 9, that the subbarrier Coulomb corrections increase the momentum shift along the propagation direction $\langle p_k \rangle$, while the continuum one oppositely decreasing it, which is in accordance with Ref. [24].

VII. CONCLUSION

We have developed a nondipole CCSFA theory and an improved simple man's model, which include Coulomb

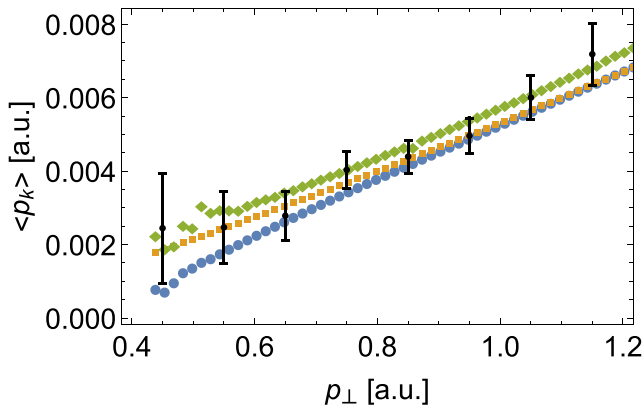


FIG. 9. The average of the longitudinal momentum vs the transverse momentum: CCSFA (blue dots), plain SFA (orange dots), CCSFA with only subbarrier corrections (green dots), and the experimental data (black points) of Ref. [5].

corrections during the subbarrier dynamics and in the continuum up to first order in E_0/E_a , the improved simple man's model includes nonadiabatic corrections up to first order in γ . Both CCSFA and simple man's model are applied for the description of the time-resolved (attoclock angle-resolved) nondipole longitudinal dynamics. Further, we have introduced the light-front momentum, which absorbs the trivial relativistic correlation between the transverse and longitudinal momenta and allows to elucidate the role of nonadiabatic and Coulomb effects. Our conclusion is that in the quasistatic regime the plain SFA and the simple man's model describe quite well the time-resolved nondipole longitudinal dynamics because of a partial compensation of the subbarrier and the continuum Coulomb effects. In contrast, the nonadiabatic Coulomb effects, especially large at small ellipticity values, introduce a deviation of the simple man's model and the plain SFA with respect to the full CCSFA. In particular, the nonadiabatic Coulomb effect in the continuum violates the symmetry of the light-front momentum with respect to the sign of the attoclock offset angle. The Coulomb effect is especially conspicuous at small ellipticity $\epsilon \lesssim 0.6$ and positive offset angles, and gives rise to interest for experimental observation [see, for instance, Figs. 2(d) and 4(d)]. The same kind of CC induces a large deviation of the parameter α from the simple man's model value 1 [see, for instance, the weak-field region in Fig. 5(a)]. The parameter α describes the shift of the peak of the transverse-momentum distribution with respect to variation of the longitudinal momentum.

We find deviations of CCSFA results from the experimental data of Ref. [4] for large offset angles and large ellipticities, which indicate that there is a notable nonadiabatic Coulomb effect and/or ionization time delay still remaining not reproducible within our CCSFA based on the eikonal approximation and applicable only for soft rescatterings.

ACKNOWLEDGMENT

We thank P.-L. He for useful discussions and R. Dörner and B. Willenberg for providing experimental data.

APPENDIX A: TRANSVERSE NONADIABATIC COULOMB MOMENTUM TRANSFER

Here we provide an intuitive estimation of the CC in the direction transverse to the laser electric field in the polarization plane in the nondipole regime. Due to nonadiabaticity the electron obtains a transverse momentum during tunneling:

$$\delta p_{yi} = \frac{\epsilon\gamma\kappa}{6}, \quad (\text{A1})$$

where the y axis is transverse to the field in the polarization plane. The Coulomb momentum transfer can be estimated as

$$\delta p_{yC} \sim \frac{Z}{x^2} \frac{y}{x} \delta t, \quad (\text{A2})$$

where x is the coordinate along the laser electric field direction, y is the transverse displacement, and δt is the effective interaction time with the atomic core. As $x \sim E_0 \delta t^2/2$, the effective time can be estimated as

$$\delta t \sim \sqrt{\frac{x_0}{E_0}}, \quad (\text{A3})$$

assuming during this time the electron displacement is twice the distance of the tunnel exit $x_0 \sim \frac{I_p}{E_0}$. The transverse displacement is

$$y \sim p_{yi} \delta t + \int^{\delta t} dt' \int^{t''} dt'' E_y(t'') = p_{yi} \delta t + \frac{\omega E_0 \delta t^3}{6}, \quad (\text{A4})$$

where $E_y \sim \epsilon E_0 \omega t$ is the transverse nonadiabatic force. The first term is estimated as

$$\sim \frac{\epsilon\gamma\kappa}{6} \frac{2ZE_0}{\kappa E_a}, \quad (\text{A5})$$

and the second one as

$$\sim E_0 \frac{\omega \delta t^3}{6} \sim \frac{\epsilon\gamma\kappa}{6} \frac{2ZE_0}{\kappa E_a}. \quad (\text{A6})$$

Thus,

$$\delta p_{yC} \sim \frac{\epsilon\gamma\kappa}{6} \frac{4Z}{\kappa} \frac{E_0}{E_a}. \quad (\text{A7})$$

APPENDIX B: LONGITUDINAL COULOMB MOMENTUM TRANSFER

Here we provide an intuitive estimation of the CC in the laser propagation direction in the nondipole regime, when the electron has an initial momentum at the tunnel exit p_{ki} . The Coulomb momentum transfer can be estimated as

$$\delta p_{kC} \sim \frac{Z}{x^2} \frac{z}{x} \delta t. \quad (\text{B1})$$

We estimate the longitudinal displacement:

$$z \sim p_{ki} \delta t + \int \frac{p_{\perp}(t')}{c} E(t') dt' \sim p_{zi} \delta t + \frac{E_0^2 \delta t^3}{6c}. \quad (\text{B2})$$

Thus,

$$\delta p_{kC} \sim \frac{Z}{x_0^3} p_{zi} \delta t + \frac{Z}{x_0^3} \frac{E_0^2 \delta t^3}{6c}. \quad (\text{B3})$$

The first term is estimated as

$$\sim p_{ki} \frac{2ZE_0}{\kappa E_a}, \quad (\text{B4})$$

and the second one as

$$\sim \frac{I_p}{3c} \frac{2ZE_0}{\kappa E_a}. \quad (\text{B5})$$

Taking into account that $p_{ki} = \frac{I_p}{3c}$, we have

$$\delta p_{kC} \sim p_{ki} \frac{4Z}{\kappa} \frac{E_0}{E_a}. \quad (\text{B6})$$

APPENDIX C: TRANSVERSE- AND LONGITUDINAL-MOMENTUM CORRELATION

Here we provide an alternative derivation of the coefficient α related to the correlation of the transverse- and longitudinal-component momentum. We solve the electron equations of motion in the laser field of magnetic dipole approximation, with a time-dependent electric and magnetic field:

$$x''(t) = \frac{A'_x(t)}{\Lambda}, \quad (\text{C1})$$

$$y''(t) = \frac{A'_y(t)}{\Lambda}, \quad (\text{C2})$$

$$z''(t) = \frac{x'(t)A'_y(t)}{c\Lambda} - \frac{y'(t)A'_x(t)}{c\Lambda}, \quad (\text{C3})$$

with the initial conditions $x'(t_i) = v_{xi}$, $y'(t_i) = v_{yi}$, $z'(t_i) = p_{zi}$, and $x(t_i) = y(t_i) = z(t_i) = 0$. The correction to the electron final momentum due to the electric quadrupole correction to the laser field is calculated perturbatively:

$$\Delta p_x = -\frac{1}{c} \int A_x(s) z(s) ds = -\frac{E_0}{c\omega} p_{zi} \sin(\omega t_i), \quad (\text{C4})$$

$$\Delta p_y = -\frac{1}{c} \int A_y(s) z(s) ds = \frac{\epsilon E_0}{c\omega} p_{zi} \cos(\omega t_i). \quad (\text{C5})$$

The final transverse momentum is

$$p_{\perp}(p_{zi}) = \sqrt{[v_{xi} - A_x(t_i) + \Delta p_x]^2 + [v_{yi} - A_y(t_i) + \Delta p_y]^2}, \quad (\text{C6})$$

which we expand over the initial longitudinal momentum p_{zi} around p_{z0} :

$$\begin{aligned} \alpha_{\theta} &\equiv \frac{p_{\perp}(p_{zi})}{\epsilon E_0/c\omega} \\ &= \{\epsilon \cos(\omega t_i) [c v_{yi} \omega + \epsilon E_0 (c + p_{z0}) \cos(\omega t_i)] \\ &\quad - c v_{xi} \omega \sin(\omega t_i) + E_0 (c + p_{z0}) \sin^2(\omega t_i)\} \frac{1}{\epsilon} \\ &\quad \times \{c^2 (v_{xi}^2 + v_{yi}^2) \omega^2 + E_0 (c + p_{z0}) [\epsilon \cos(\omega t_i) (2c v_{yi} \omega \end{aligned}$$

$$\begin{aligned}
& + \epsilon E_0(c + p_{z0}) \cos(\omega t_i) - 2c v_{xi} \omega \sin(\omega t_i) \\
& + E_0(c + p_{z0}) \sin^2(\omega t_i) \}^{-1/2}. \quad (C7)
\end{aligned}$$

For the values for v_{xi} , and v_{yi} , we use Eqs. (31), and for p_{z0} , Eq. (32). The results for α_θ with this estimation coincide with those in Figs. 4.

- [1] C. T. L. Smeenk, L. Arissian, B. Zhou, A. Mysyrowicz, D. M. Villeneuve, A. Staudte, and P. B. Corkum, Partitioning of the Linear Photon Momentum in Multiphoton Ionization, *Phys. Rev. Lett.* **106**, 193002 (2011).
- [2] A. Ludwig, J. Maurer, B. W. Mayer, C. R. Phillips, L. Gallmann, and U. Keller, Breakdown of the Dipole Approximation in Strong-Field Ionization, *Phys. Rev. Lett.* **113**, 243001 (2014).
- [3] J. Maurer, B. Willenberg, J. Daněk, B. W. Mayer, C. R. Phillips, L. Gallmann, M. Klaiber, K. Z. Hatsagortsyan, C. H. Keitel, and U. Keller, Probing the ionization wave packet and recollision dynamics with an elliptically polarized strong laser field in the nondipole regime, *Phys. Rev. A* **97**, 013404 (2018).
- [4] B. Willenberg, J. Maurer, B. W. Mayer, and U. Keller, Sub-cycle time resolution of multi-photon momentum transfer in strong-field ionization, *Nat. Commun.* **10**, 5548 (2019).
- [5] A. Hartung, S. Eckart, S. Brennecke, J. Rist, D. Trabert, K. Fehre, M. Richter, H. Sann, S. Zeller, K. Henrichs *et al.*, Magnetic fields alter strong-field ionization, *Nat. Phys.* **15**, 1222 (2019).
- [6] N. Haram, I. Ivanov, H. Xu, K. T. Kim, A. Atia-tul Noor, U. S. Sainadh, R. D. Glover, D. Chetty, I. V. Litvinyuk, and R. T. Sang, Relativistic Nondipole Effects in Strong-Field Atomic Ionization at Moderate Intensities, *Phys. Rev. Lett.* **123**, 093201 (2019).
- [7] S. Grundmann, D. Trabert, K. Fehre, N. Strenger, A. Pier, L. Kaiser, M. Kircher, M. Weller, S. Eckart, L. P. H. Schmidt, F. Trinter, T. Jahnke, M. S. Schöffler, and R. Dörner, Zeptosecond birth time delay in molecular photoionization, *Science* **370**, 339 (2020).
- [8] A. Hartung, S. Brennecke, K. Lin, D. Trabert, K. Fehre, J. Rist, M. S. Schöffler, T. Jahnke, L. P. H. Schmidt, M. Kunitski, M. Lein, R. Dörner, and S. Eckart, Electric Nondipole Effect in Strong-Field Ionization, *Phys. Rev. Lett.* **126**, 053202 (2021).
- [9] K. Lin, S. Brennecke, H. Ni, X. Chen, A. Hartung, D. Trabert, K. Fehre, J. Rist, X.-M. Tong, J. Burgdörfer, L. P. H. Schmidt, M. S. Schöffler, T. Jahnke, M. Kunitski, F. He, M. Lein, S. Eckart, and R. Dörner, Magnetic-Field Effect in High-Order Above-Threshold Ionization, *Phys. Rev. Lett.* **128**, 023201 (2022).
- [10] K. Lin, S. Eckart, A. Hartung, D. Trabert, K. Fehre, J. Rist, L. P. H. Schmidt, M. S. Schöffler, T. Jahnke, M. Kunitski, and R. Dörner, Photoelectron energy peaks shift against the radiation pressure in strong field ionization, [arXiv:2110.04027](https://arxiv.org/abs/2110.04027).
- [11] N. Haram, H. Xu, I. Ivanov, D. Chetty, I. Litvinyuk, and R. T. Sang, Strong field ionisation of Argon: Electron momentum spectra and nondipole effects, *Phys. Rev. A* **105**, 023522 (2022).
- [12] K. Lin, X. Chen, S. Eckart, H. Jiang, A. Hartung, D. Trabert, K. Fehre, J. Rist, L. P. H. Schmidt, M. S. Schöffler, T. Jahnke, M. Kunitski, F. He, and R. Dörner, Magnetic-Field Effect as a Tool to Investigate Electron Correlation in Strong-Field Ionization, *Phys. Rev. Lett.* **128**, 113201 (2022).
- [13] M. Klaiber, E. Yakaboylu, H. Bauke, K. Z. Hatsagortsyan, and C. H. Keitel, Under-the-Barrier Dynamics in Laser-Induced Relativistic Tunneling, *Phys. Rev. Lett.* **110**, 153004 (2013).
- [14] S. Chelkowski, A. D. Bandrauk, and P. B. Corkum, Photon Momentum Sharing Between an Electron and an Ion in Photoionization: From One-Photon (Photoelectric Effect) to Multiphoton Absorption, *Phys. Rev. Lett.* **113**, 263005 (2014).
- [15] D. Cricchio, E. Fiordilino, and K. Z. Hatsagortsyan, Momentum partition between constituents of exotic atoms during laser-induced tunneling ionization, *Phys. Rev. A* **92**, 023408 (2015).
- [16] S. Chelkowski, A. D. Bandrauk, and P. B. Corkum, Photon-momentum transfer in multiphoton ionization and in time-resolved holography with photoelectrons, *Phys. Rev. A* **92**, 051401(R) (2015).
- [17] I. A. Ivanov, Relativistic calculation of the electron-momentum shift in tunneling ionization, *Phys. Rev. A* **91**, 043410 (2015).
- [18] I. A. Ivanov, J. Dubau, and K. T. Kim, Nondipole effects in strong-field ionization, *Phys. Rev. A* **94**, 033405 (2016).
- [19] A. S. Simonsen, T. Kjellsson, M. Førre, E. Lindroth, and S. Selstø, Ionization dynamics beyond the dipole approximation induced by the pulse envelope, *Phys. Rev. A* **93**, 053411 (2016).
- [20] S. Chelkowski, A. D. Bandrauk, and P. B. Corkum, Photon-momentum transfer in photoionization: From few photons to many, *Phys. Rev. A* **95**, 053402 (2017).
- [21] T. Keil and D. Bauer, Coulomb-corrected strong-field quantum trajectories beyond dipole approximation, *J. Phys. B: At., Mol. Opt. Phys.* **50**, 194002 (2017).
- [22] J. F. Tao, Q. Z. Xia, J. Cai, L. B. Fu, and J. Liu, Coulomb rescattering in nondipole interaction of atoms with intense laser fields, *Phys. Rev. A* **95**, 011402(R) (2017).
- [23] P.-L. He, D. Lao, and F. He, Strong Field Theories Beyond Dipole Approximations in Nonrelativistic Regimes, *Phys. Rev. Lett.* **118**, 163203 (2017).
- [24] P.-L. He, M. Klaiber, K. Z. Hatsagortsyan, and C. H. Keitel, Nondipole coulomb sub-barrier ionization dynamics and photon momentum sharing, *Phys. Rev. A* **105**, L031102 (2022).
- [25] J. Ullrich, R. Moshhammer, A. Dorn, R. Dörner, L. P. H. Schmidt, and H. Schmidt-Böcking, Recoil-ion and electron momentum spectroscopy: reaction-microscopes, *Rep. Prog. Phys.* **66**, 1463 (2003).
- [26] A. Di Piazza, C. Müller, K. Z. Hatsagortsyan, and C. H. Keitel, Extremely high-intensity laser interactions with fundamental quantum systems, *Rev. Mod. Phys.* **84**, 1177 (2012).
- [27] V. I. Ritus, Quantum effects of the interaction of elementary particles with an intense electromagnetic field, *J. Sov. Laser Res.* **6**, 497 (1985).
- [28] B. Wolter, M. G. Pullen, M. Baudisch, M. Scalfani, M. Hemmer, A. Senftleben, C. D. Schröter, J. Ullrich, R. Moshhammer, and J. Biegert, Strong-Field Physics With Mid-Ir Fields, *Phys. Rev. X* **5**, 021034 (2015).
- [29] M. Dammasch, M. Dörr, U. Eichmann, E. Lenz, and W. Sandner, Relativistic laser-field-drift suppression of nonsequential multiple ionization, *Phys. Rev. A* **64**, 061402(R) (2001).
- [30] M. C. Kohler, T. Pfeifer, K. Z. Hatsagortsyan, and C. H. Keitel, Chapter 4 - Frontiers of atomic high-harmonic generation, *Adv. At. Mol. Phys.* **61**, 159 (2012).

- [31] M. Klaiber, K. Z. Hatsagortsyan, J. Wu, S. S. Luo, P. Grugan, and B. C. Walker, Limits of Strong Field Rescattering in the Relativistic Regime, *Phys. Rev. Lett.* **118**, 093001 (2017).
- [32] M. Førre, J. P. Hansen, L. Kocbach, S. Selstø, and L. B. Madsen, Nondipole Ionization Dynamics of Atoms in Superintense High-Frequency Attosecond Pulses, *Phys. Rev. Lett.* **97**, 043601 (2006).
- [33] C. Liu and K. Z. Hatsagortsyan, Coulomb focusing in above-threshold ionization in elliptically polarized midinfrared strong laser fields, *Phys. Rev. A* **85**, 023413 (2012).
- [34] J. Daněk, M. Klaiber, K. Z. Hatsagortsyan, C. H. Keitel, B. Willenberg, J. Maurer, B. W. Mayer, C. R. Phillips, L. Gallmann, and U. Keller, Interplay between coulomb-focusing and non-dipole effects in strong-field ionization with elliptical polarization, *J. Phys. B: At., Mol. Opt. Phys.* **51**, 114001 (2018).
- [35] J. Daněk, K. Z. Hatsagortsyan, and C. H. Keitel, Analytical approach to coulomb focusing in strong-field ionization. i. nondipole effects, *Phys. Rev. A* **97**, 063409 (2018).
- [36] J. Daněk, K. Z. Hatsagortsyan, and C. H. Keitel, Analytical approach to coulomb focusing in strong-field ionization. ii. multiple recollisions, *Phys. Rev. A* **97**, 063410 (2018).
- [37] B. Willenberg, J. Maurer, U. Keller, J. Daněk, M. Klaiber, N. Teeny, K. Z. Hatsagortsyan, and C. H. Keitel, Holographic interferences in strong-field ionization beyond the dipole approximation: The influence of the peak and focal-volume-averaged laser intensities, *Phys. Rev. A* **100**, 033417 (2019).
- [38] J. Maurer and U. Keller, Ionization in intense laser fields beyond the electric dipole approximation: concepts, methods, achievements and future directions, *J. Phys. B: At., Mol. Opt. Phys.* **54**, 094001 (2021).
- [39] H. Ni, S. Brennecke, X. Gao, P.-L. He, S. Donsa, I. Březinová, F. He, J. Wu, M. Lein, X.-M. Tong, and J. Burgdörfer, Theory of Subcycle Linear Momentum Transfer in Strong-Field Tunneling Ionization, *Phys. Rev. Lett.* **125**, 073202 (2020).
- [40] N. Haram, R. T. Sang, and I. V. Litvinyuk, Transverse electron momentum distributions in strong-field ionization: Nondipole and coulomb focusing effects, *J. Phys. B: At., Mol. Opt. Phys.* **53**, 154005 (2020).
- [41] Y. Ma, J. Zhou, P. Lu, H. Ni, and J. Wu, Influence of nonadiabatic, nondipole and quantum effects on the attoclock signal, *J. Phys. B: At., Mol. Opt. Phys.* **54**, 144001 (2021).
- [42] M. M. Lund and L. B. Madsen, Nondipole photoelectron momentum shifts in strong-field ionization with mid-infrared laser pulses of long duration, *J. Phys. B: At., Mol. Opt. Phys.* **54**, 165602 (2021).
- [43] S. Brennecke and M. Lein, Nondipole modification of the ac stark effect in above-threshold ionization, *Phys. Rev. A* **104**, L021104 (2021).
- [44] P. B. Corkum, Plasma perspective on strong field multiphoton ionization, *Phys. Rev. Lett.* **71**, 1994 (1993).
- [45] M. Klaiber, E. Yakaboylu, and K. Z. Hatsagortsyan, Above-threshold ionization with highly charged ions in superstrong laser fields. I. Coulomb-corrected strong-field approximation, *Phys. Rev. A* **87**, 023417 (2013).
- [46] M. Klaiber, E. Yakaboylu, and K. Z. Hatsagortsyan, Above-threshold ionization with highly charged ions in superstrong laser fields. II. Relativistic Coulomb-corrected strong-field approximation, *Phys. Rev. A* **87**, 023418 (2013).
- [47] M. Klaiber, K. Z. Hatsagortsyan, and C. H. Keitel, Gauge-invariant relativistic strong-field approximation, *Phys. Rev. A* **73**, 053411 (2006).
- [48] M. Klaiber, K. Z. Hatsagortsyan, and C. H. Keitel, Above-threshold ionization beyond the dipole approximation, *Phys. Rev. A* **71**, 033408 (2005).
- [49] M. Klaiber, K. Z. Hatsagortsyan, and C. H. Keitel, Tunneling Dynamics in Multiphoton Ionization and Attoclock Calibration, *Phys. Rev. Lett.* **114**, 083001 (2015).
- [50] N. Shvetsov-Shilovski, S. Goreslavski, S. Popruzhenko, and W. Becker, Capture into rydberg states and momentum distributions of ionized electrons, *Laser Phys.* **19**, 1550 (2009).
- [51] A. M. Perelomov, V. S. Popov, and V. M. Terent'ev, Ionization of atoms in an alternating electric field II, *Zh. Exp. Theor. Fiz.* **51**, 309 (1966) [*Sov. Phys. JETP* **24**, 207 (1967)].
- [52] M. V. Ammosov, N. B. Delone, and V. P. Krainov, Tunnel ionization of complex atoms and of atomic ions in an alternating electromagnetic field, *Zh. Eksp. Theor. Fiz.* **91**, 2008 (1986) [*Sov. Phys. JETP* **64**, 1191 (1986)].